Prediction of the transparency in the visible range of x-ray absorbing nanocomposites built upon the assembly of LaF3 or LaPO4 nanoparticles with poly(methyl methacrylate)

Fady El Haber, Xavier Rocquefelte, Christine Andraud, Bouhalouane Amrani, Stéphane Jobic, Olivier Chauvet, Gerard Froyer

Prediction of the transparency in the visible range of x-ray absorbing nanocomposites built upon the assembly of LaF_3 or $LaPO_4$ nanoparticles with poly(methyl methacrylate)

Fady El Haber,[1,*] Xavier Rocquefelte,[1,4] Christine Andraud,[2] Bouhalouane Amrani,[3] Stéphane Jobic,[1] Olivier Chauvet,[1] and Gérard Froyer[1]

[1]*Institut des Matériaux Jean Rouxel (IMN), Université de Nantes, CNRS, 2 rue de la Houssinière, BP 32229, 44322 Nantes Cedex 03, France*

[2]*Institut des NanoSciences de Paris (INSP) UMR-CNRS 7588, Université Pierre et Marie Curie, Paris VI, 4 place Jussieu, F-75252 Paris Cedex 05, France*

[3]*Laboratoire de Physique des Couches Minces et Matériaux pour l'Electronique (LPC2ME), Université d'Oran, Es-sénia, Oran 31000, Algeria*

[4]*Xavier.rocquefelte@cnrs-imn.fr*

**Corresponding author: Fady.elhaber@cnrs-imn.fr*

A theoretical multiscale approach combining density functional theory and four-flux calculations based on the radiative transfer theory is used to prospect the optical properties of nanocomposite materials composed of in-organic nanoparticles of lanthanum-containing compounds (LaF_3 or $LaPO_4$) embedded in Poly(methyl methacry-late) (PMMA). This theoretical investigation shows that a potential route to produce lead-free x-ray shielding screens with high transparency in the visible range (>70% of incident light) may consist in incorporating colorless LaF_3 or $LaPO_4$ spherical particles with a diameter lower than 6 nm in a PMMA panel from a minimum thickness of 3 mm with a volumetric fraction of at least 10%. In terms of x-ray attenuation, this would lead to lead equivalency of 0.1 mm (lead foil).

1. INTRODUCTION

During the past few years, lanthanum trifluoride (LaF_3) and lanthanum phosphate ($LaPO_4$) nanoparticles (NPs) have been extensively investigated as antiwear materials [1], polymer fillers or lubricating grease additives [2,3], and host lattices for luminescent properties [4–10]. Recently, El Haber and Froyer also showed that these materials also exhibit remarkable properties for protection against x-ray radiation [11]. Hence, these compounds, once embedded in a highly transparent organic matrix such as the poly(methyl methacrylate) (PMMA), can be regarded as potential substitutes for lead-containing glasses. Such an alternative has great merit both to respect the European directives in terms of toxicology [12] and to lighten the protective devices, making easy their manipulation. However, the challenge remains so far to achieve a good compromise between the x-ray absorbing capacity and the high transparency of the x-ray shield to envision applications in the medical domain, for instance.

Very preliminary investigations carried out on ball-milled PMMA/LaF_3 or PMMA/$LaPO_4$ powdered mixtures with 10% volume of 6 nm large NPs exhibit a lead equivalency of 0.1 mm for x-ray attenuation for 3 mm thick white pellets. Based on this result, specific synthetic routes were developed for the elaboration of LaF_3 and lanthanum orthophosphate NPs with modified surfaces to favor their dispersion in PMMA by dispersing surface modified NPs in methyl methacrylate monomer for radical polymerization [13]. Nevertheless, if $LaPO_4$ and LaF_3 in PMMA may be envisioned in the future as efficient x-ray shielding system in the 38–80 keV energy domains [11], some prerequisites are expected before commercialization. Hence, in addition to the x-ray absorption capabilities, such screens must exhibit for applications in the radiology department (Fig. 1) a high transparency in the visible range to facilitate the observation of the patient by the x-ray manipulator throughout the examination. For this reason, a light transmission higher than 70% in the visible range (380–800 nm) of the x-ray shielding panel is requested.

The aim of the present paper is to predict the transparency properties of such nanocomposite material in the visible range using a multiscale theoretical approach, taking into account the refractive index of the inorganic particles but also their size, their concentration in the organic medium, the thickness of the x-ray attenuator, etc. Namely, after analyzing the intrinsic optical properties of $LaPO_4$ and LaF_3 based on first-principles calculations, the refractive indices and the extinction coefficients of these two compounds were extracted and used as input parameters in four-flux calculations to shed light on the extrinsic optical properties of the nanocomposites (i.e., $LaPO_4$ or LaF_3 embedded in PMMA) materials.

2. THEORETICAL APPROACH

A. Our Strategy

In general, the light interaction with nanocomposites can be roughly estimated via the Beer–Lambert law for highly diluted

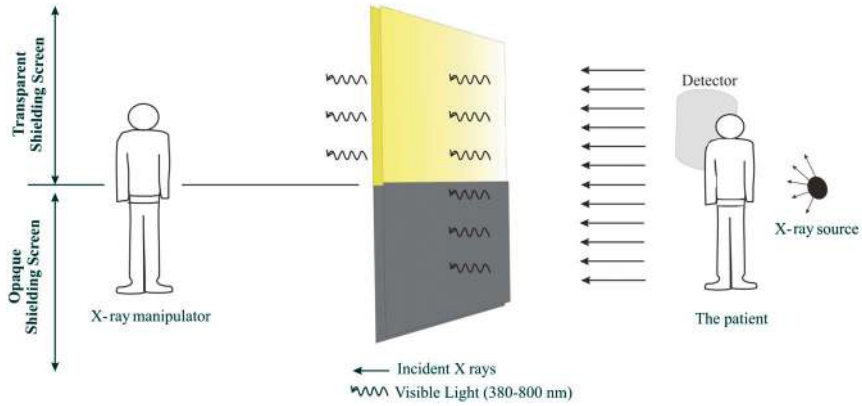

Fig. 1. X-ray shielding structure used in radiology departments where the x-ray manipulator has to be protected against x rays in everyday life. The transparent x-ray shield (upper part) should transmit at least 70% of visible light with lead equivalency of 0.1 mm

systems. When the concentration in the scattering centers increased, multiple scattering phenomena appear and cannot be neglected. Namely, the electromagnetic light scattering is a complex phenomenon because of the existence of secondary radiations dissipating energy in all directions. Therefore, the total scattered light depends strongly on the relative size of the particles compared to the incident wavelength and how these particles are dispersed in the matrix with respect to the incident light and scattered directions [14].

In case of diluted media, for well-separated small particles, single-scattering approximation can be used [15,16]. However, in the present case, the scattering medium contains a large number of particles. As a consequence, the single-scattering approximation is no longer valid, and multiple scattering phenomena have to be taken into account, which implies solving the radiative transfer equation (RTE) [17]. Considering that there is no interference between the radiation scattered by neighboring particles [18], the resolution of the RTE leads to four-flux calculations to estimate transparency properties of nanocomposites. To carry out such radiative transfer calculations, few inputs are needed: the optical constants (refractive index and extinction coefficient) of the organic medium and light scatterers, the shape of the scattering centers (here supposed to be spherical), their size and their concentration, and the thickness of the medium to pass through.

B. Intrinsic Optical Properties—Density Functional Theory Calculations

An accurate description of the optical properties of LaF_3 and $LaPO_4$ bulk compounds may be achieved via a quantum mechanical treatment. Namely, both scattering and absorption properties of an insulating compound are related to the dielectric function $\varepsilon(\omega) = \varepsilon_1(\omega) + i\varepsilon_2(\omega)$, which describes the linear response of the electronic structure to the electric field of the impinging light carrying an $\hbar\omega$ energy [19,20]. The spectral dependence of the optical properties can be theoretically determined from the electronic band structure by calculating the $\varepsilon_2(\omega)$ spectrum, which is related to the capacity of the material to absorb light [20]. The $\varepsilon_1(\omega)$ function is then obtained using the Kramers–Kronig relations [21]. It should be noted that, in contrast to the treatment of experimental optical data, no extrapolations are necessary to perform the integrals in the Kramers–Kronig analysis in the present DFT calculations due to an estimation of the ε_2 values for a high energy range. Finally, the complex refractive index, $N(\omega) = n(\omega) + ik(\omega)$, could be deduced from $\varepsilon_1(\omega)$ and $\varepsilon_2(\omega)$ using the following formulas:

$$n(\omega) = \frac{(\varepsilon_1(\omega) + (\omega_1^2(\omega))^{0.5})^{0.5}}{\sqrt{2}}, \tag{1a}$$

$$k(\omega) = \frac{(-\varepsilon_1(\omega) + (\omega_1^2(\omega) + \omega_2^2(\omega))^{0.5})^{0.5}}{\sqrt{2}}, \tag{1b}$$

where $n(\omega)$ and $k(\omega)$ are the refractive index and the extinction coefficient at a given optical angular frequency of the incoming radiation, respectively. These two quantities, used as input in the four-flux calculations, will be determined here on the basis of DFT calculations using the WIEN2k program package [22].

In order to correctly describe the position of the very localized $4f$ states of La^{3+} ions ($4f^\circ$ electronic configuration) and the related optical properties, we have carried out DFT calculations within the generalized gradient approximation (GGA) [23] plus on-site Coulomb repulsion (U). The validity of the GGA + U approach has been tested by changing the value of the effective Hubbard parameter, $U_{\text{eff}} = U - J$, where J is the Hund's exchange interaction, the U value being determined by trial and error. As will be discussed in Subsection 3.A, a U_{eff} value of about 10.3 eV has been shown to provide a coherent picture both in terms of x-ray photoelectron spectroscopy (XPS) combined with bremsstrahlung isochromat spectroscopy (BIS) and reflectivity spectroscopy of LaF_3.

The density of states and optical properties are deduced from a self-consistent calculation, using the full-potential linearized augmented plane-wave method, as embodied in the WIEN2k code. The maximum l value in the expansion of the basis set inside the atomic sphere was 12. The convergence of the basis set is controlled by a cutoff parameter $\text{RMT} \times K_{\max} = 7$, where RMT is the smallest atomic sphere radius in the unit cell and $K_{\max}$ is the magnitude of the largest k vector. The self-consistency was carried out on a 32 k-point mesh in the irreducible Brillouin zone, with the following radii: RMT(La) = 2.3 *a.u.*, RMT(F) = 2.1 *a.u.*, RMT(P) = 1.67 *a.u.*, RMT(O) = 1.2 *a.u.*, and GMAX = 12 bohr^{-1}, where GMAX is the magnitude of the largest vector in the charge density Fourier expansion.

C. Extrinsic Optical Properties—Four-Flux Calculations

It is important to note that materials under consideration consist of NPs dispersed in PMMA (Fig. 2). To ensure a good transparency to the nanocomposite, light scattering caused by the NPs must be minimized as described in the Rayleigh scattering equation [Eq. (2)]. Namely, scattering phenomena is enhanced when the diameter (D_p) and the volumetric concentration of the inorganic particles in the matrix increase (short interparticles r distances) but can be minimized when n_p/n_m tends to 1:

$$I_R = \frac{8\pi^4 n_m D_p^6}{\lambda^4 r^2}\left|\frac{\left(\frac{n_p}{n_m}\right)^2 - 1}{\left(\frac{n_p}{n_m}\right)^2 + 2}\right|(1+\cos\theta)I_0, \qquad (2)$$

the Rayleigh scattering equation where I_R and I_0 are the scattered and the incident intensities, respectively, D_p the particle diameter, λ the wavelength, r the distance between the particles, and θ the scattering angle. n_p/n_m is the refractive indices ratio of the inorganic particles (n_p) and the organic medium (n_m).

Namely, the RTE [Eq. (3)] accounts for both the simple scattering and the multiple one. Emission phenomena are not considered at all in this type of analysis:

$$\frac{dI}{ds} = \underset{\text{single scattering}}{\underset{\uparrow}{-(\alpha_{abs}+\alpha_{sca})I}} + \underset{\text{multiple scattering}}{\underset{\uparrow}{\alpha_{sca}\int_{4\pi} p\cdot I' d\omega'}}, \qquad (3)$$

the RTE where I is the intensity of radiation, p the phase function depending on the angular distribution of scattered light, $\alpha_{sca} = NC_{sca}$ the scattering coefficient (N = number of inorganic inclusions in the organic medium per volume unit), and $\alpha_{abs} = NC_{abs}$ the absorption coefficient (C_{sca} and C_{abs} are the scattering and absorption cross sections, respectively, calculated by Mie theory).

This four-flux model was phenomenologically established by Maheu and Gouesbet [15]. The solution of Eq. 3 gives access to the values of the four fluxes, that is, the specular and the scattered reflected beams (hereafter labeled Rcc and Rcd, respectively) and the specular and the scattered transmitted beam (hereafter labeled Tcc and Tcd, respectively) [24,25] (Fig. 2).

The multiple reflections inside the layer are taken into account with the Fresnel coefficient for the collimated beam, and for scattered beam, the diffuse reflection coefficient is calculated using an angular average over all angles of incidence of the Fresnel reflection coefficient $r(\theta)$ (where θ is the angle of incidence of the light), considering that the scattered beam is isotropic. To gain simplicity, it should be noticed that, in our calculations, the following restrictions have been considered: (i) incident light is supposed to be monochromatic light with a quasi-constant electric field; (ii) the scattering light has the same frequency as the incident light; and (iii) the medium surrounding the NPs is homogeneous, linear, isotropic and nonabsorbing (i.e., PMMA).

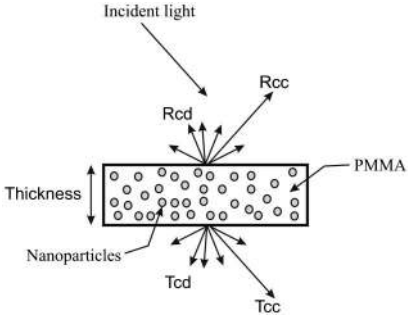

Fig. 2. Schematic representation of the interaction of light with an x-ray absorbing panel built upon inorganic NPs embedded in PMMA (Rcc, specular reflectance; Rcd, scattered reflectance; Tcc, specular transmission; Tcd, scattered transmission).

3. RESULTS AND DISCUSSION

A. Intrinsic Optical Properties—LaF_3 and $LaPO_4$ Bulk Compounds

In order to extract the refractive indices and extinction coefficients of LaF_3 and $LaPO_4$, we have estimated the optical properties of these two compounds in their bulk configuration based on DFT calculations. Before discussing these results, we first consider the effect of the U_{eff} and scissors-operator (SO) parameters on the electronic structure of LaF_3. The on-site U_{eff} parameter will be taken the same for $LaPO_4$ (see below).

The total densities of states of LaF_3 obtained using GGA, GGA + U and GGA + U + SO are represented in Fig. 3. In the present case, a Gaussian broadening has been applied to the theoretical density of states (DOS) in order to reproduce the experimental broadening related to XPS and BIS experiments of LaF_3 [26]. To have a proper description of the optical properties of these two compounds, it was necessary to apply two corrections. The first one consists in applying a Hubbard term (U_{eff} = 10.3 eV) to the 4f(La) states in order to have a more localized description of these levels and then an adequate position of the energy levels. The second one consists in having a proper description of the bandgap of these two compounds. There are several ways of correcting this DFT deficiency [26], the simplest one being to use an SO, i.e., shifting the conduction bands rigidly with respect to the valence bands to have a bandgap similar to the experimental one (SO = 2 and 1.8 eV for $LaPO_4$ and LaF_3, respectively).

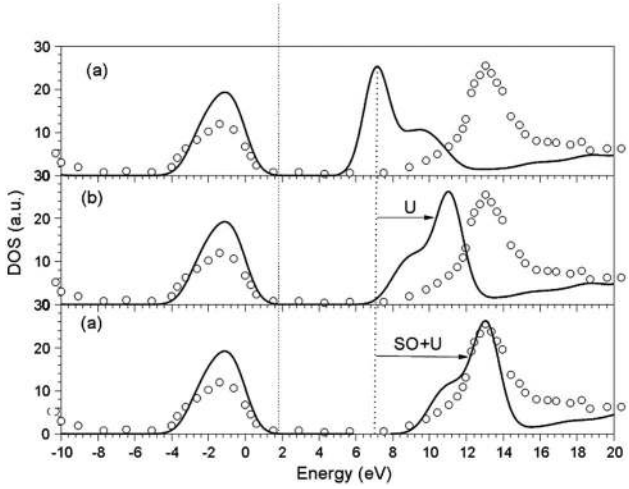

Fig. 3. Comparison of the total densities of states of LaF_3 deduced from (a) GGA, (b) GGA + U, and (c) GGA + U + SO approaches. The open circles correspond to the XPS/BIS experimental data [26].

It should be noticed that, in contrast to the correction of the bandgap, which is system dependent, the U_{eff} value is expected to be the same for LaF_3 and $LaPO_4$ due to the atomiclike nature of the $4f$(La) states, in a first approximation.

The general features of these three calculated DOSs given in Fig. 3 are similar except a significant change of the La($4f$) band positions as a function of the U_{eff} value and of the bandgap as a function of the SO value. Figures 3a and 3b show the effect of applying a Hubbard term ($U_{\text{eff}} = 10.3$ eV). However, while the correction of the $4f$(La) position using GGA + U allows us to have a proper description of the shape of the BIS (related to the conduction band) and the XPS (related to the valence band) spectra, it does not provide a good description of the bandgap value, as expected. The final result is then obtained using GGA + U + SO and shown in Fig. 3c, leading to good agreements with the reported XPS/BIS experimental data [27].

In summary, the electronic structure of LaF_3 could be described as follows. Below the Fermi level, the occupied bands are mainly composed of $2p$(F) states interacting with $5d$(La) states. Above the Fermi level, the first empty states are mainly composed of $5d$(La) states, and the $4f$(La) states are inside the $5d$(La) block and not in the bandgap, as found in GGA calculations. This observation has a strong impact in terms of the understanding of the optical properties of LaF_3: at low energy, the optical properties will be mainly controlled by the $2p(F) \rightarrow 5d$(La) optical transitions.

Figures 4a and 4b compare the measured reflectivity at normal incidence on a basal plane of LaF_3 [28] to the simulation deduced from GGA and GGA + U calculations. In the two cases, the simulations before and after applying the SO are provided. The arrow in Fig. 4a shows the optical transitions involving the $4f$(La) states and that are not expected at such low energy. In contrast, using GGA + U + SO approach allows having a proper description of the LaF_3 reflectivity curve up to energy of 20 eV, at least. Such an observation confirms the validity of the present approach to properly describe the optical properties of LaF_3. It should be noticed that the SO for $LaPO_4$ (SO = 2 eV) has been chosen in such a way to reproduce its experimental optical gap of 7.8 eV [29]. Calculated band structure of $LaPO_4$ is not given here but compares well with the one determined by Mishra *et al.* [30].

Extinction coefficient (k) and refractive index (n) values for these two compounds could then be extracted from the present GGA + U + SO calculations. Figures 5a and 5b represent k and n, respectively, for LaF_3 and $LaPO_4$. The present calculations evidenced that $LaPO_4$ and LaF_3 start absorbing light at about 7.8 and 10 eV, respectively. As expected, these

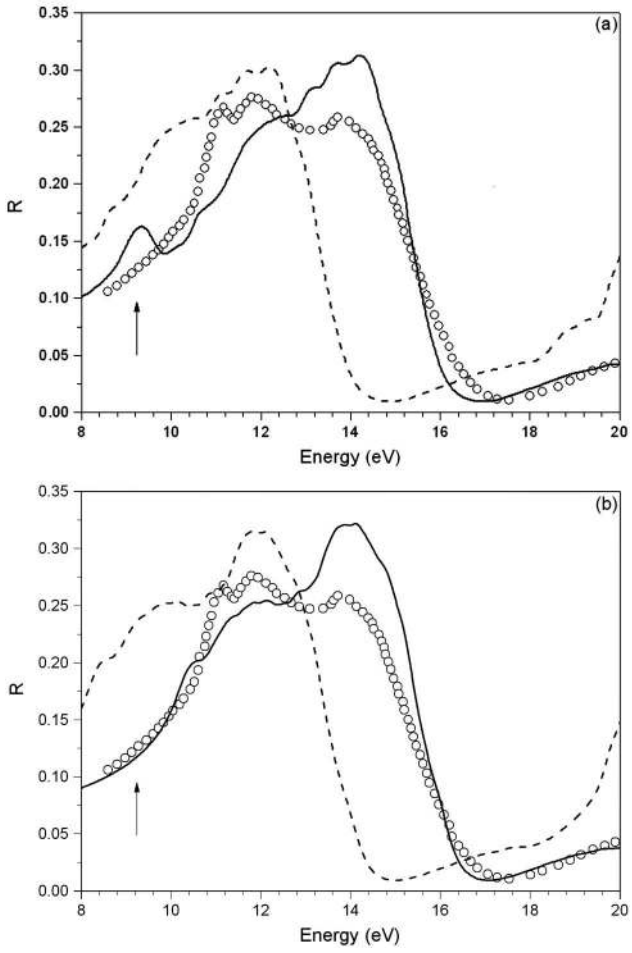

Fig. 4. Experimental [28] (open circles) and theoretical reflectance spectra of LaF_3: (a) simulations deduced from GGA (dashed line) and GGA + SO (solid line), (b) simulations deduced from GGA + U (dashed line) and GGA + U + SO (solid line). The arrow indicates the region that is incorrectly simulated by the GGA + SO approach due to an underestimation of the $4f$(La) energy.

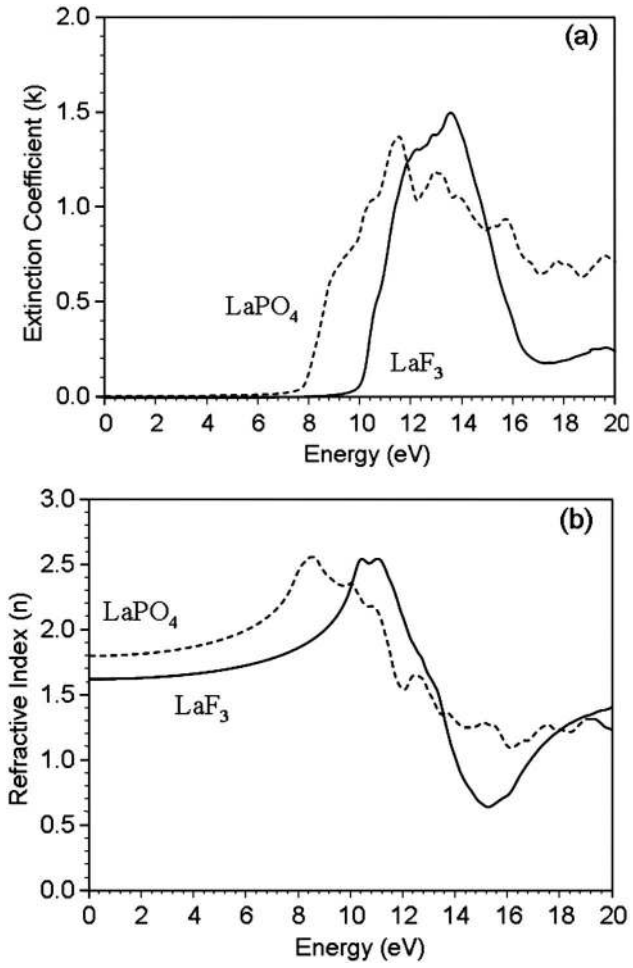

Fig. 5. (a) Theoretical extinction coefficients and (b) refractive indices of LaF_3 and $LaPO_4$ deduced from GGA + U + SO calculations.

two compounds are intrinsically transparent in the visible light range (1.55–3.1 eV), i.e., no absorption occurs in the 380–800 nm domain. In addition, it should be noticed that the high bandgap value implies a resulting small refractive index value in the visible range, due to the causality rule that links k and n, expressed by the Kramers–Kronig relation. In fact, the refractive indices deduced from our DFT calculations in the energy window (1.55–3.1 eV) ranged from 1.80 to 1.84 for $LaPO_4$ and 1.62 to 1.64 for LaF_3, in accordance with the experimental measurements [31,32].

To gain simplicity, the refractive indices of LaF_3 and $LaPO_4$ would be taken constant on the whole visible range, i.e., 1.62 and 1.82, respectively, while k would be settled to zero.

B. Extrinsic Optical Properties—Nanocomposite Materials

To anticipate the transparency properties of LaF_3 and $LaPO_4$ NPs in PMMA and to direct the preparation of x-ray absorber/polymer composites with the requisites for medical applications, for instance, simulations of the optical characteristics in the visible range were carried out by the four-flux method with a special calculation code developed by Institute of Nanoscience in Paris, France [33]. The refractive index of PMMA (n_{PMMA}) was taken equal to 1.49 [34]. The thickness (e) of the x-ray shield was taken at 3 mm or more, and the volume percentage of NP in polymer (vol. %) was equal or higher than 10% to ensure a sufficient absorption of x ray. By reference with preliminary synthetic investigations [13], particle size was taken around 6 nm.

Figure 6 displays the evolution of light transmission [$T(\lambda)$] versus the nanocomposite thickness (e) along the whole visible range for spherical absorbing particle with 6 nm diameters. We can clearly notice that the thickness in the 3–5 mm domain (step of 0.5 mm) does not impact significantly the transparency of the materials even if a more pronounced decrease of $T(\lambda)$ is observed for wavelengths lower than

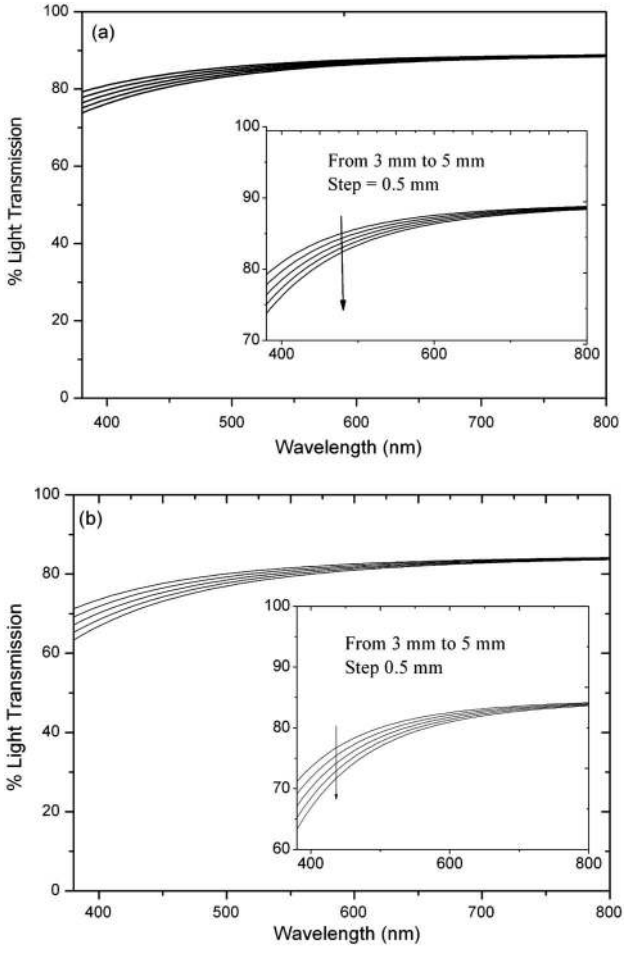

Fig. 6. Evolution of the total transmission (Tcc + Tcd) versus the thickness e of the x-ray absorbing layer for e ranging from 3 to 5 mm ($D_p = 6$ mm, vol. % = 10%). (a) LaF_3 NPs $n_p = 1.62$; (b) $LaPO_4$ NPs $np = 1.8$.

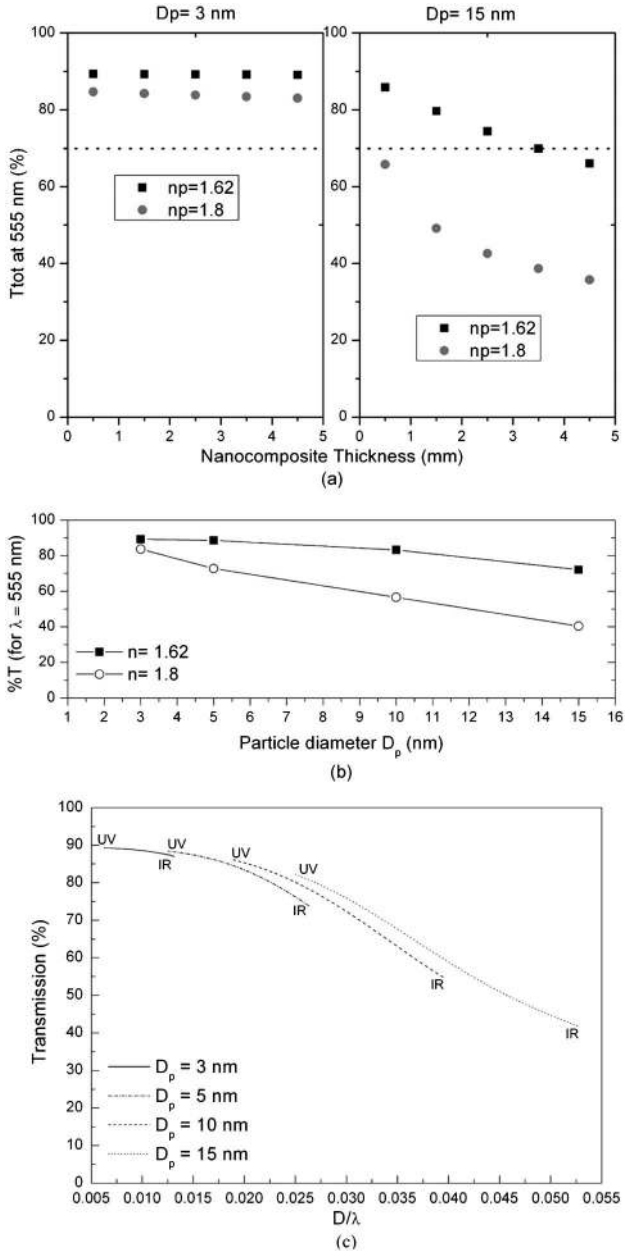

Fig. 7. (a) Transmission at 555 nm of x-ray attenuators whose thickness ranges from 0.5 to 5 mm for LaF_3 and $LaPO_4$ NPs embedded in PMMA (volume fraction of 10%). (Left) $D_p = 3$ nm; (Right) $D_p = 15$ nm. (b) Transmission at 555 nm versus inorganic NP diameters a 3 mm thick x-ray shield (volume fraction of NPs = 10%). (c) Light transmission of LaF_3/PMMA x-ray attenuator versus D_p/λ (where $\lambda = 380$–800 nm) ratio for particle diameters of 3, 5, 10 and 15 nm ($e = 3$ mm, vol. % = 10).

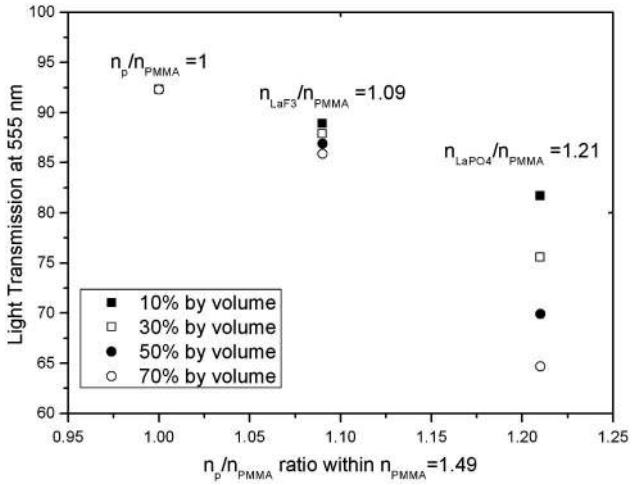

Fig. 8. Light transmission variation with the np/n_{PMMA} ratio for LaF_3 and $LaPO_4$ NPs for volume fraction ranging from 10% to 70% ($e = 3$ mm, $D_p = 6$ mm).

600 nm. Namely, for LaF_3/PMMA nanocomposite, light transmission shifts from 88.9% to 88.4% at 800 nm and from 79.3% to 73.8% at 380 nm going from $e = 3$ mm to $e = 5$ mm. For $LaPO_4$/PMMA composites, the transparency is less than with LaF_3 due to a higher refractive index of the scattering centers. The transmission shifts then from 84.1% to 83.6% at 800 nm and from 71.2% to 63.3% at 380 nm for $e = 3$ mm and $e = 5$ mm, respectively. Nevertheless, transmission remains higher than 70% for any compositions at 555 nm, i.e., the wavelength corresponding to the maximum photopic sensitivity of the eyes. This means that LaF_3/PMMA and $LaPO_4$/PMMA composites may be convenient to replace 0.1 mm lead equivalency foils to protect against x ray while insuring a good transparency in the visible range.

To evidence the role of the size particle of the scattering particles, Fig. 7a depicts the evolution of transparency at 555 nm for layers whose thickness changes from 0.5 to 5 mm. Calculations were carried out with LaF_3 and $LaPO_4$ NPs with diameter of 3 and 15 nm for a constant volume percentage of 10%. While it turns out that transmission at 555 nm is almost not impacted by panel thickness for particle size of 3 nm, $T(555\,\mathrm{nm})$ falls down very fast with (e) for 15 nm diameter particles. The higher the particle size, the lower the transparency of the absorbing panel for a given thickness, at least for $D_p \ll \lambda$. This is well illustrated in Figs. 7a and 7b, while Fig. 7c represents the evolution of the transmission versus D_p/λ in the UV–visible–IR domain for LaF_3 and $LaPO_4$ NPs at vol. $\% = 10\%$ in PMMA, for $e = 3$ mm.

Let consider now the evolution of $T(555$ nm) for LaF_3 and $LaPO_4$ 6 nm diameter NPs in PMMA for different volume percentages of the inorganic phase for a panel thickness of 3 mm. Figure 8 shows the $T(555)$ versus n_p/n_{PMMA} for volumetric concentration of 10%, 30%, 50%, and 70%. It appears clearly that the higher the n_p/n_{PMMA} ratio, the higher the negative impact of an increase of the particle/polymer volumetric ratio. Namely, $T(555\,\mathrm{nm})$ shifts from 90% to 85% and from 83% to 63% when n_p/n_{PMMA} increases from 1.09 to 1.21 going from LaF_3 to $LaPO_4$. For a reminder, $T(555\,\mathrm{nm})$ remains constant and equal to 93% for a particle with the same refractive index as the medium. The attenuation of the intensity of the passing beam is observed because particles hit by the impinging beam act as scattering centers emitting radiation in any direction. In particular, it clearly appears that a way to overcome the transmission light decrease when the refractive index of the inorganic particle is increased is to reduce significantly the diameter of the inorganic particle. In the present case, with particles diameters of 5 nm and less, the use of inorganic compounds with a refractive index up to 1.9 will do not induce too strong an opacity of the nanocomposite material. In contrast with particles having a diameter higher than 5 nm, the opacity will be strongly dependent of the refractive index value of the particle.

4. CONCLUSION

To conclude, the present theoretical investigation has provided a way to estimate the impact of intrinsic and extrinsic parameters on the optical properties of a nanocomposite material composed of inorganic inclusions (LaF_3 and $LaPO_4$) embedded in an organic medium (PMMA). More specifically, the role of the extrinsic parameters n_p/n_m and D_p/λ have been discussed based on a multiscale approach combining DFT and four-flux calculations. After validating our DFT results based on comparison with XPS/BIS and reflectivity experimental data, the intrinsic optical characteristics of LaF_3 and $LaPO_4$ have been extracted and used as input parameters in the four-flux calculations. Our results provide the magnitude of the light transmission reduction when n_p/n_m deviates from 1 and when D_p/λ is raised (impact of the multiple scattering). In particular to avoid too strong an opacity of a panel composed of such nanocomposite material with PMMA as the organic medium, the use of LaF_3 has to be more privileged than $LaPO_4$ because it provides an n_p/n_m ratio closer to 1. Whatever, if we limit our analysis to a 3 mm thick shield with a 10 vol. % inorganic absorber concentration to ensure 0.1 mm lead equivalency of protection against x rays, NPs of a size lower than 6 nm should be sufficient to lead transmission higher than 70%. Let us notice that another strategy allowing the insertion of particles with a larger size would consist in the use of an organic medium with a higher refractive index, that is polystyrene ($n_m = 1.55$) in place of PMMA ($n_m = 1.49$), for instance.

REFERENCES

1. J. Zhou, Z. Wu, Z. Zhang, W. Liu, and H. Dang, "Synthesis and room temperature ionic conductivity of nano-LaF_3 bulk material," Wear **249**, 333–337 (2001).
2. R. Dekker, V. Sudarsan, F. C. J. M. van Veggel, K. Wörhoff, and A. Driessen, *Proceedings Symposium IEEE/LEOS Benelux Chapter* (IEEE, 2004).
3. J. W. Stouwdam and F. C. J. M. van Veggel, "Near-infrared emission of redispersible Er^{3+}, Nd^{3+}, and Ho^{3+} doped LaF_3 nanoparticles," Nano Lett. **2**, 733–737 (2002).
4. T. Grzyb and S. Lis, "Photoluminescent properties of LaF_3:Eu^{3+} and GdF_3:Eu^{3+} nanoparticles prepared by co-precipitation method," J. Rare Earth **27**, 588–592 (2009).
5. D. Pi, F. Wang, X. Fan, M. Wang, and Y. Zhang, "Luminescence behavior of Eu^{3+} doped LaF_3 nanoparticles," Spectrochim. Acta A **61**, 2455–2459 (2005).
6. M. A. Lim, S. I. Seog, W. J. Chung, and S. I. Hong, "Near infrared luminescence properties of nanohybrid film prepared from $LaPO_4$:Er^{3+}/$LaPO_4$ core/shell nanoparticles and silica-based resin," Opt. Mater. **31**, 201–205 (2008).
7. H.-K. Jung, J.-S. Oh, S.-I. Seok, and T.-H. Lee, "Preparation and luminescence properties of $LaPO_4$:Er, Yb nanoparticles," J. Lumin. **114**, 307–313 (2005).

8. W. Yan, Q. Weiping, Z. Jisen, and C. Chunyan, "Role of organic molecules on upconversion luminescence of LaF_3 nanoparticles," Mater. Lett. **63**, 1285–1288 (2009).
9. Y. Wei, F. Lu, X. Zhang, and D. Chen, "Polyol-mediated synthesis of water-soluble LaF_3:Yb, Er upconversion fluorescent nanocrystals," Mater. Lett. **61**, 1337–1340 (2007).
10. M.-Y. Xie, L. Yu, H. He, and X.-F. Yu, "Synthesis of highly fluorescent LaF_3Ln^{3+}/LaF_3 core/shell nanocrystals by a surfactant-free aqueous solution route," J. Solid State Chem. **182**, 597–601 (2009).
11. F. El Haber and G. Froyer, "Transparent polymers embedding nanoparticles for x-rays attenuation," J. Univ. Chem. Technol. Metall. **43**, 283–290 (2008).
12. The RoHS Regulation, Directive 2002/95/EC, http://www.rohs.eu.
13. F. El Haber, "Contribution à l'obtention de verres organiques sans plomb atténuateurs des rayons X- Synthèse modification de surface et caractérisations de nanoparticules incorporables dans les polymères acryliques" Ph.D thesis (Université de Nantes, 2007).
14. M. Mishchenko, L. D. Travis, and A. A. Lacis, *Scattering, Absorption, and Emission of Light by Small Particles* (NASA Goddard Institute for Space Studies, 2004).
15. B. Maheu and G. Gouesbet, "Four-flux models to solve the scattering transfer equation: special cases," Appl. Opt. **25**, 1122–1128 (1986).
16. B. Maheu, J. N. Le Toulouzan, and G. Couesbet, "Four-flux models to solve the scattering transfer equation in terms of Lorenz–Mie parameters," Appl. Opt. **23**, 3353–3362 (1984).
17. J.-C. Auger, B. Stout, and J. Lafait, "Dependent light scattering in dense heterogeneous media," Physica B **279**, 21–24 (2000).
18. G. A. Niklasson, "Comparison between four flux theory and multiple scattering theory," Appl. Opt. **26**, 4034–4036 (1987).
19. W. D. Lynch, *Interband Absorption-Mechanisms and Interpretations—Handbook of Optical Constants of Solids*, E. D. Palik, ed. (Academic, 1985).
20. F. Bassani and G. P. Parravicini, *Electronic States and Optical Transitions in Solids*, R. A. Ballinger, ed. (Pergamon, 1975).
21. C. Ambrosch-Draxl and J. Sofo, "Linear optical properties of solids within the full-potential linearized augmented plane wave method," Comput. Phys. Commun. **175**, 1–14 (2006).
22. P. Blaha, K. Schwarz, G. Madsen, D. Kvasnicka, and J. Luitz, *WIEN2k: An Augmented Plane Wave+LO Program for Calculating Crystal Properties* (TUW, 2001).
23. J. P. Perdew, K. Burke, and M. Ernzerhof, "Generalized gradient approximation made simple," Phys. Rev. Lett. **77**, 3865–3868 (1996).
24. W. E. Vargas, "Generalized four-flux radiative transfer model," Appl. Opt. **37**, 2615–2623 (1998).
25. C. Rozé, T. Girasole, G. Gréhan, G. Gouesbet, and B. Maheu, "Average crossing parameter and forward scattering ratio values in four-flux model for multiple scattering media," Opt. Commun. **194**, 251–263 (2001).
26. K.-H. Park and S.-J. Oh, "Electron-spectroscopy study of rare-earth trihalides," Phys. Rev. B **48**, 14833–14842 (1993).
27. K. Held, V. I. Anisimov, V. Eyert, G. Keller, A. K. McMahan, I. A. Nekrasov, and D. Vollhardt, "LDA + DMFT investigations of transition metal oxides and f-electron materials," Adv. Solid State Phys. **43**, 267–286 (2003).
28. C. G. Olson, M. Piacentini, and D. W. Lynch,"Optical properties of single crystals of some rare-earth trifluorides, 5–34 eV," Phys. Rev. B **18**, 5740–5749 (1978).
29. E. Nakzawa and F. J. Shiga,"Vacuum ultraviolet luminescence-excitation spectra of $RPO_4:Eu^{3+}$ ($R = Y$, La, Gd and Lu)," J. Lumin. **15**, 255–259 (1977).
30. K. C. Mishra, I. Osterloh, H. Anton, B. Hannebauer, P. C. Schmidt, and K. H. Johnson, "First principles investigation of host excitation of $LaPO_4$, La_2O_3 and $AlPO_4$," J. Lumin. **72–74**, 144–145 (1997).
31. P. Chindaudom and K. Vedam, "Determination of the optical constants of an inhomogeneous transparent LaF_3 thin film on a transparent substrate by spectroscopic ellipsometry," Opt. Lett. **17**, 538–540 (1992).
32. C. M. Gramaccioli and T. V. Segalstad, "A uranium-and thorium-rich monazite from a south-alpine pegmatite at Piona, Italy," Am. Mineral. **63**, 757–761 (1978).
33. A. Da Silva, C. Andraud, E. Charron, B. Stout, and J. Lafait, "Multiple light scattering in multilayered media: theory, experiments," Physica B **338**, 74–78 (2003).
34. O. Zieman, J. Krauser, P. E. Zamzow, and W. Daum, *POF Handbook: Optical Short Range Transmission Systems* (Springer, 2008).